

## Chapter 4 Measurements and discussions

### 4.1 Mechanical measurement

The fabrication process was completed on two SOI wafers. There was totally 32 dies with different designs; each die contained only one device and each design differed in comb finger length, finger width, and minimum finger gaps. A special design with unbalanced comb finger gaps was also included. A fabricated device is shown in Figure 4.1. The size is about  $0.7 \times 1.2 \times 1.3 \text{ cm}^3$ .

The devices were tested after releasing. Probes were used to push the center plate to verify if the devices were successfully released by HF solution as shown in Figure 4.2. The measurement setup is shown in Figure 4.3. A shaker driven by a function generator was used to drive the device. Vibration was measured by an accelerometer. The displacement is observed by an optical microscope and with a digital camera.

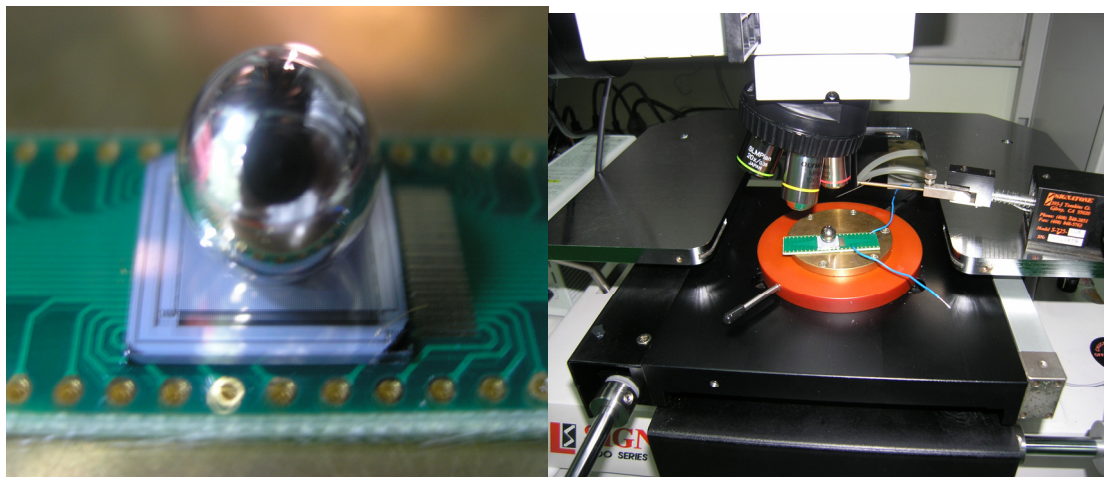
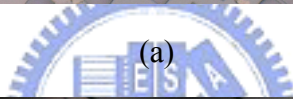
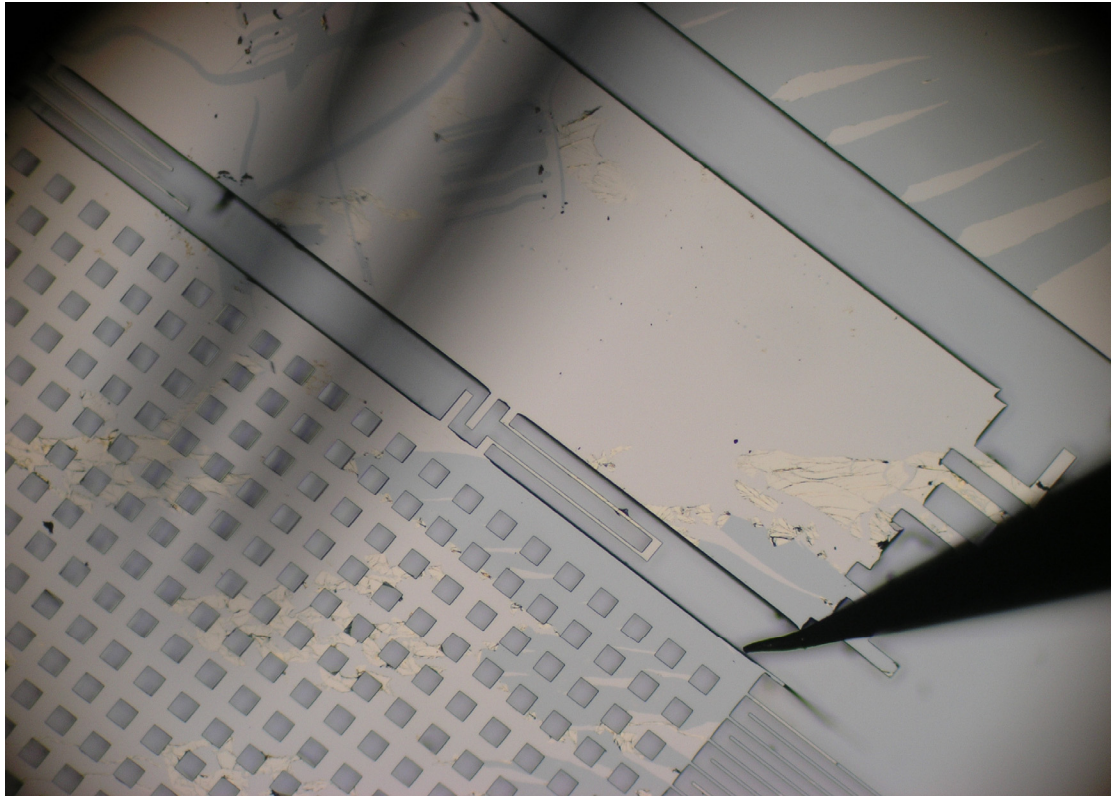
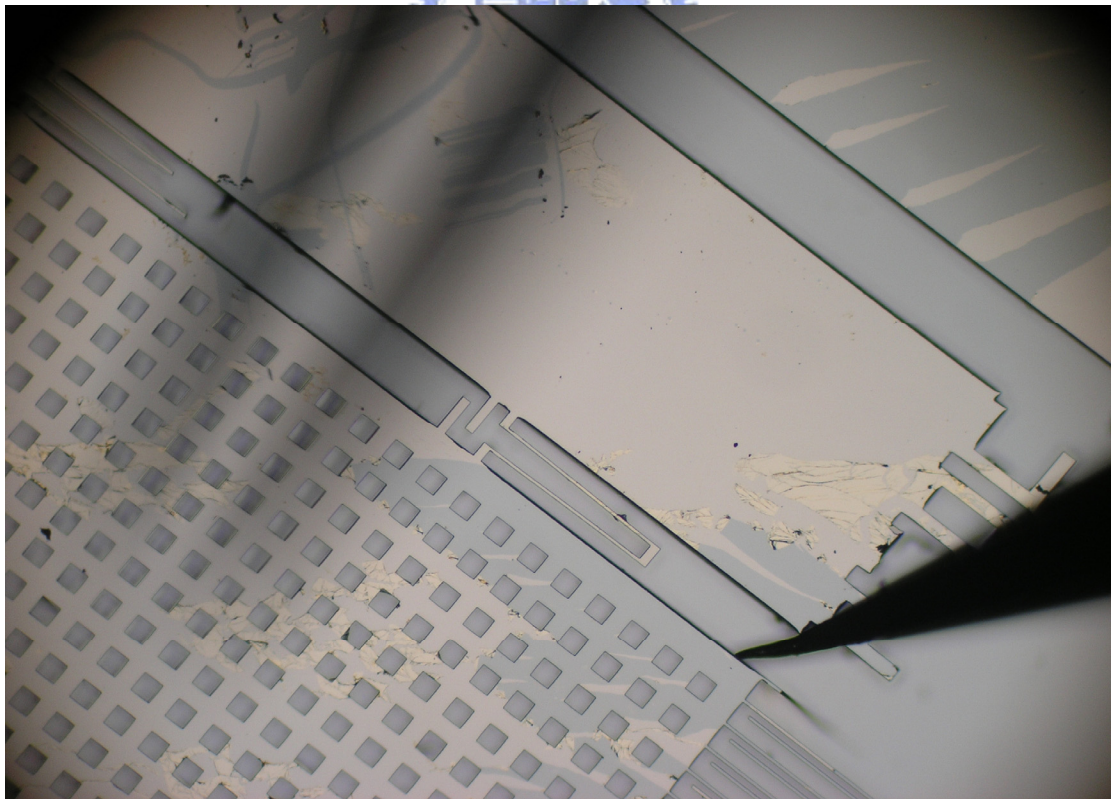


Figure 4.1 Device and the optical microscope stage



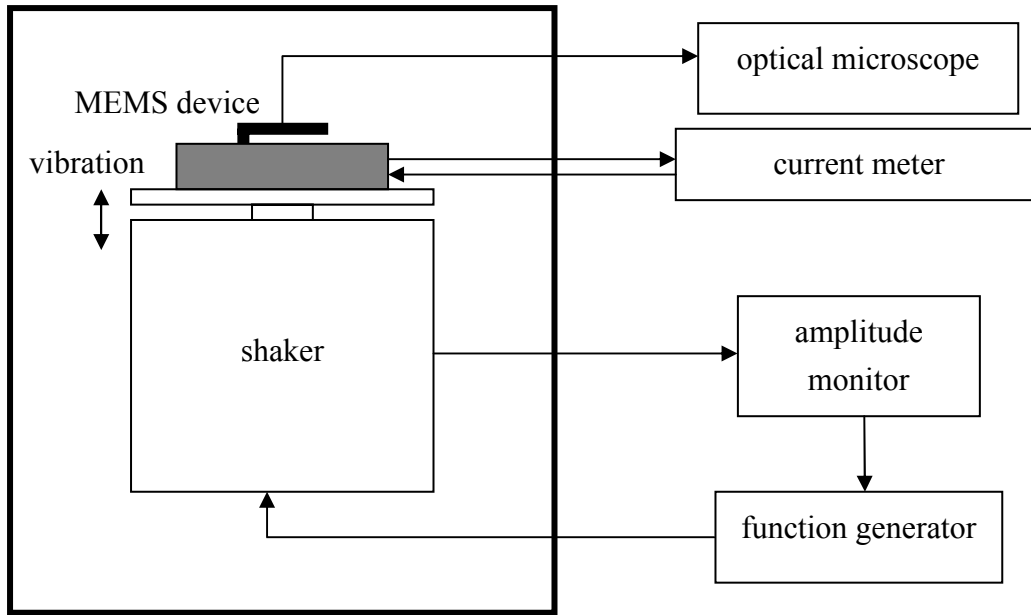
(a)



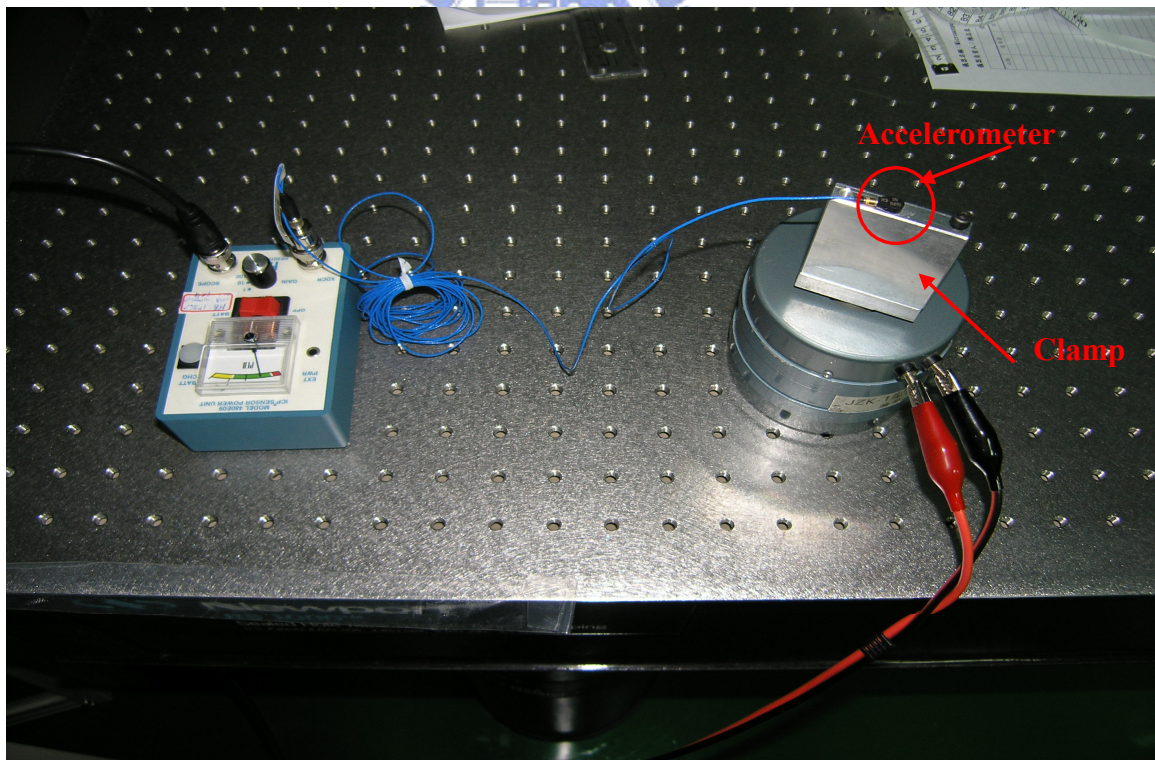
(b)

Figure 4.2 Releasing test: (a) before push (b) after push





(a)



(b)

Figure 4.3 Measurement setup (a) Schematic (b) photograph

Displacement of the device without the attached mass and without input voltage was measured as shown in Figure 4.4. Figure 4.4 (a) shows part of the comb fingers under static condition (vibration at 0 Hz), the movable finger is in the center and the fixed fingers are beside. It can be seen that the fingers in Figure 4.4(b) become blurred due to vibration. Displacement of the movable plates is estimated by comparing the blur area with the static condition. Note that the fixed fingers also become blurred since it represents the displacement of the frame of the device and also, the vibration source  $y$ . The relative displacement  $z$  is thus the displacement of movable fingers with displacement of fixed fingers subtracted. Figure 4.5 shows the measured displacement. The acceleration was  $40\text{m/s}^2$  and the vibration frequency range from 500 to 1000Hz. The maximum displacement is about  $10\mu\text{m}$  at 800Hz, and quality factor  $Q = \omega_0/\Delta\omega$  is about 9.6, where  $\omega_0$  is the resonant frequency and  $\Delta\omega$  is the bandwidth as shown in Figure 4.5. Even though the displacement was close to the pull-in limit, the pull-in effect did not occur because there was no voltage applied to the device in this test. The mass of the center plate is approximately 0.038gram, thus the spring constant calculated from the equation  $\omega = \sqrt{k/m} \Rightarrow k = \omega^2 m$  is  $960 \mu\text{N}/\mu\text{m}$ .

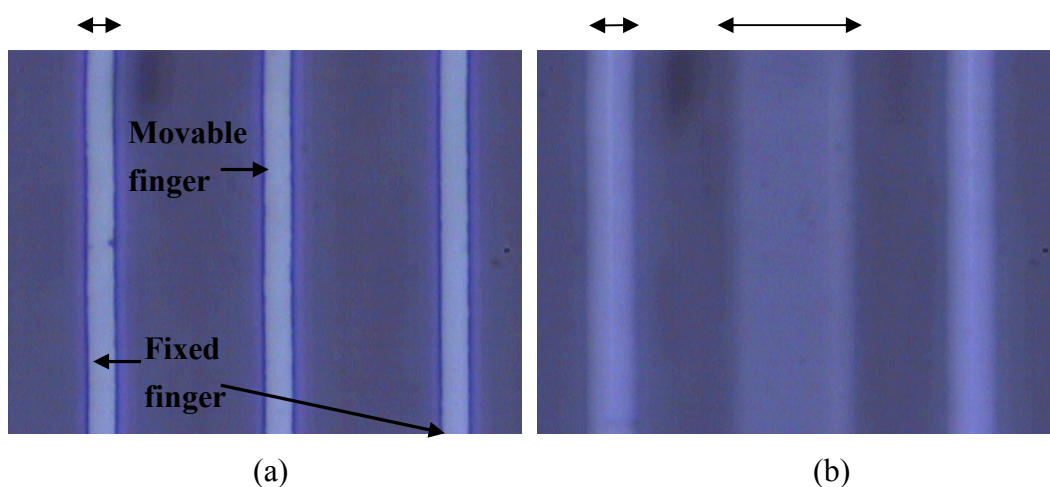


Figure 4.4 Fingers under (a) 0 Hz and (b) 800Hz vibration

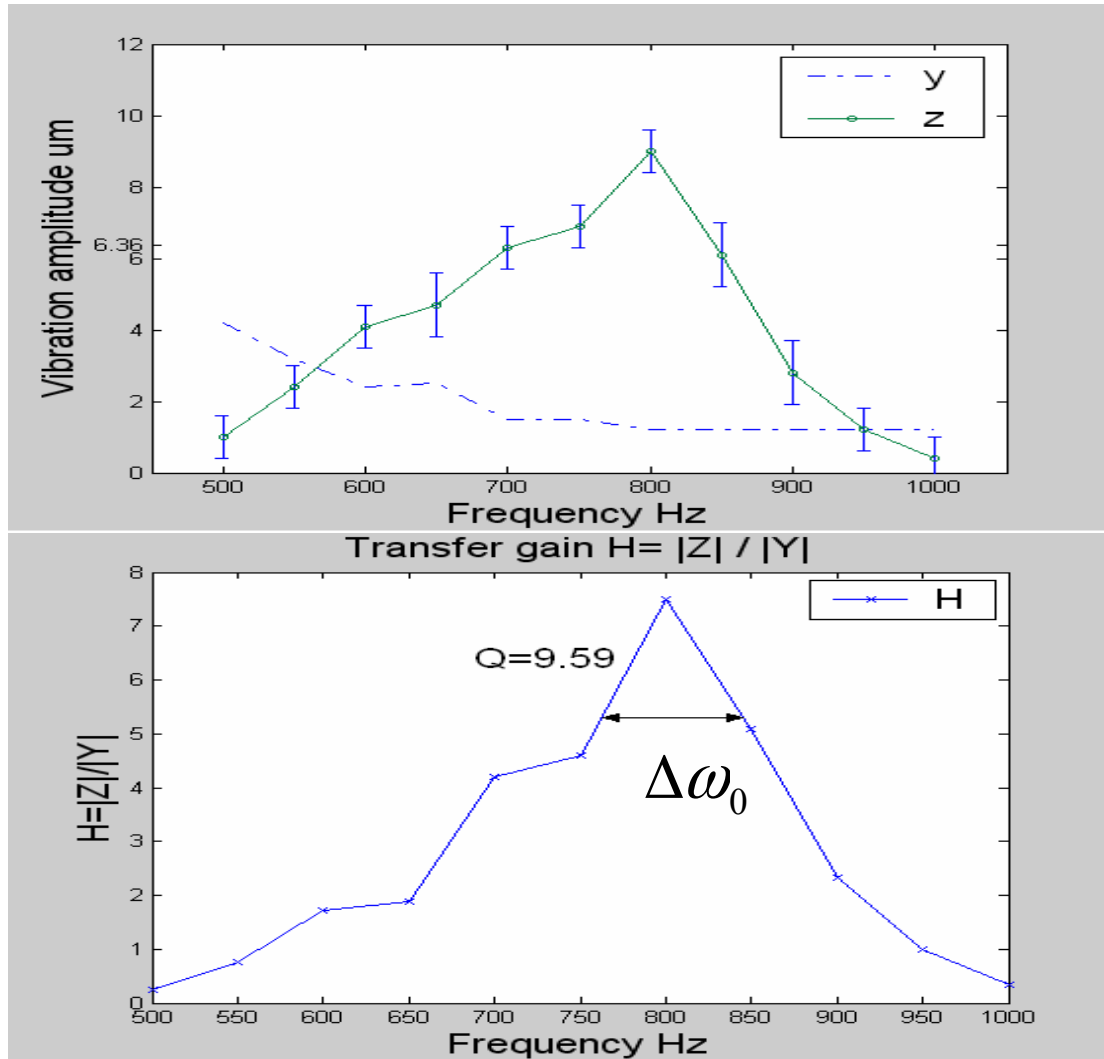


Figure 4.5 Frequency response of the device

The vertical spring constant was obtained by using the equation  $F = kx = mg$ . The sink displacement of devices with different masses was measured using an interferometer. The displacements were measured on the two ends of spring legs at the four springs on the corner of the movable plate and averaged. Measurements on three samples were conducted. The measured vertical spring constant is about  $(6 \pm 2) \times 10^5 \mu\text{N}/\mu\text{m}$ , which is about 2~3 times less than calculated value of  $1.1 \times 10^6 \mu\text{N}/\mu\text{m}$ .

The measured spring constants are different from the calculation in both the lateral and vertical directions. The major factor of the discrepancy is due to the feature size shrink in the fabrication process.

The lateral spring constant is proportional to the cube of the spring width. Figure 4.6 shows the lateral spring constant versus different spring width from 6 to 10  $\mu\text{m}$ . The SEM picture in Figure 3.10 shows the fabricated spring width shrinks from 10  $\mu\text{m}$  to about 6.8  $\mu\text{m}$ . The measured spring constant is 960  $\mu\text{N}/\mu\text{m}$ , which is very close to that of the spring width 7  $\mu\text{m}$  in Figure 4.6. Therefore, the major reason for decreased spring constant is the shrunk spring width.

The vertical spring constant is proportional to the spring width and is also plotted in Figure 4.7. The measured vertical spring constant ranging from  $4.3 \times 10^5$  to  $8.1 \times 10^5$   $\mu\text{N}/\mu\text{m}$  falls in the range of spring constant calculated with spring width of 4~7.5  $\mu\text{m}$ . The measurement error is large for that the displacement on the spring is very small (about 0.015  $\mu\text{m}$ ). But the trends also shows that the vertical spring decreased due to the spring width shrunk.

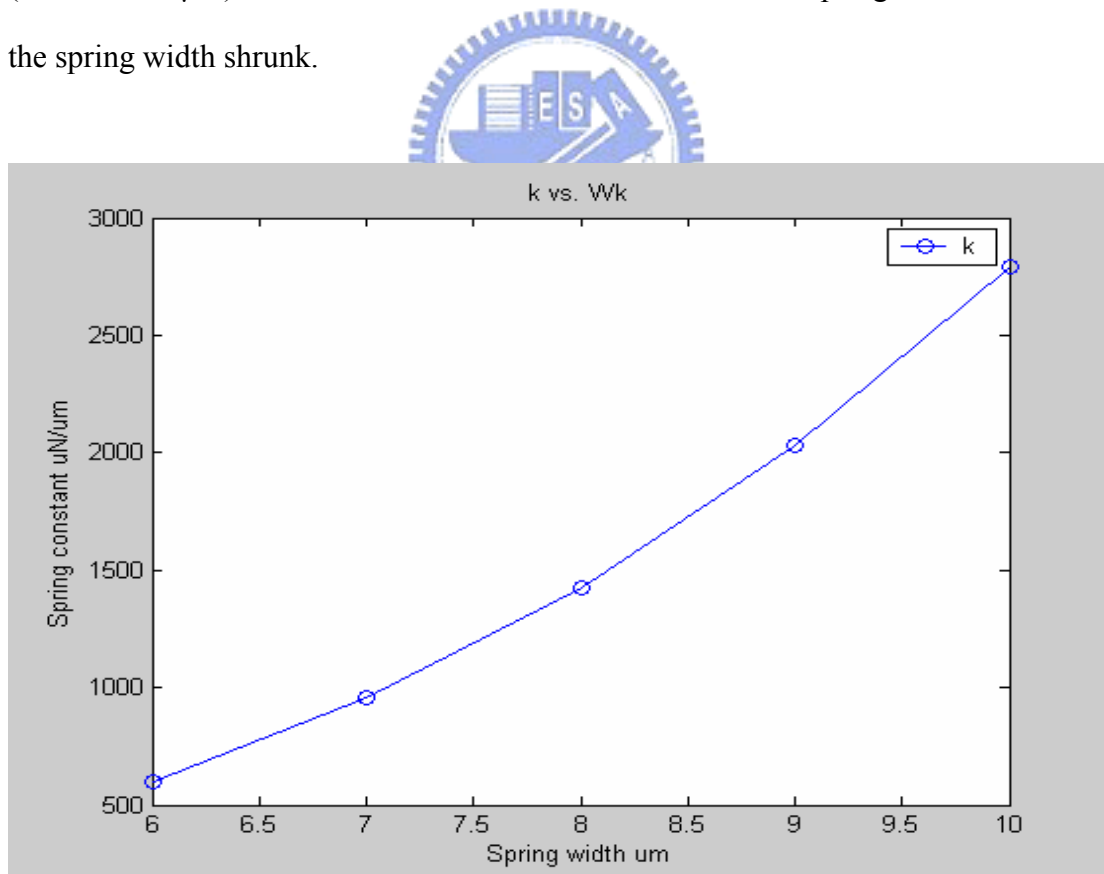


Figure 4.6 Lateral spring constant versus spring width

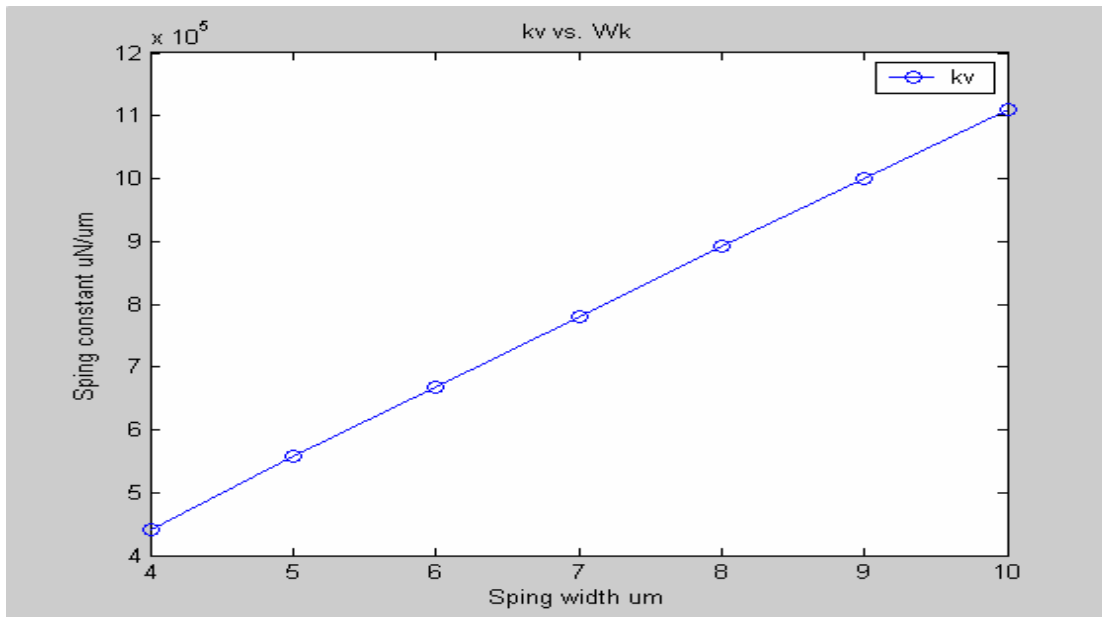


Figure 4.7 Vertical spring constant versus spring width

Modal analysis simulated by Coventorware is performed with different spring width. The first mode of spring width 8 $\mu\text{m}$  has frequency of 931Hz, and the frequency of 6 $\mu\text{m}$  width is about 491 Hz. The measured resonant frequency falls in the range of the width from 6~8 $\mu\text{m}$ . Through the above discussion, the decreased spring constant and therefore decreasing in resonant frequency ( $\omega = \sqrt{k/m}$ ) can be explained.

The displacement of devices with attached appendix mass was not measured because the devices were all broken due to external shock. The main reason is that the dynamic safety factor was not considered during the designed.

## 4.2 Electrical measurement

After the device passed the releasing test, the die was coated with aluminum of 5000 Å. And then the pads of the device were connected to the PCB board as shown in Figure 4.8. The electrical measurement was conducted using an INSTRON-LCR-816 LCR meter as shown in Figure 4.9, and HP-4192A impedance analyzer.



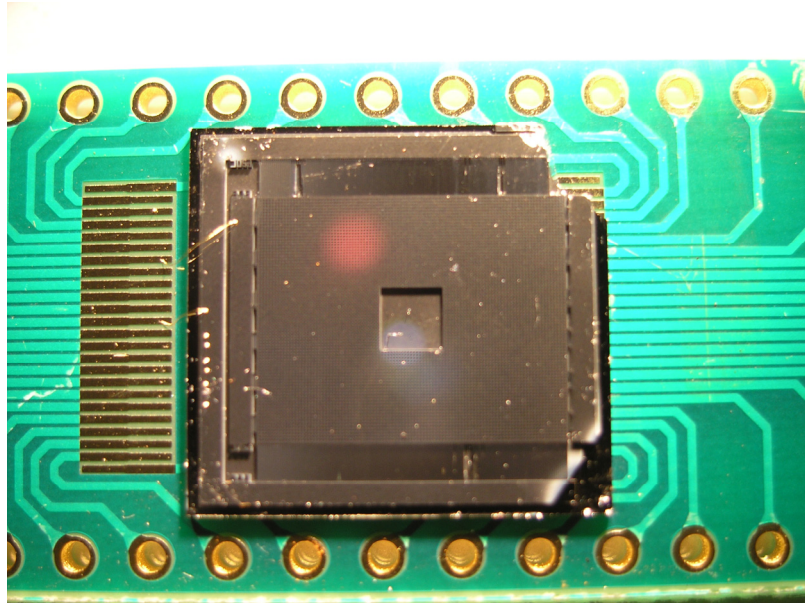


Figure 4.8 Wire bonding of device



Figure 4.9 Electrical measurement setup

The measured capacitance without vibration was about 500~600pF, while the calculated capacitance  $C_{min}$  is about 50pf. The main part of the measured capacitance is the parasitic capacitance  $C_{par}$  between the center plate and the substrate beneath it. The measured dummy parasitic capacitance of the PCB board is about 1pF, and the calculated  $C_{par}$  is about 350 pF.



Besides the parasitic capacitance, there is also a parasitic resistance. The measured resistance varies from die to die with an average resistance of 2.5 k $\Omega$ . Both the resistance and the capacitance were double checked by both the LCR meter and the impedance analyzer.

In the original design the device operation should be test and measured according to the schematic in Figure 2.1(a). A similar prototype with bare die diode attached to the MEMS variable structure as switch have been fabricated [11]. However the prototype was not functional due to leakage current and parasitic resistance and several problems. In fact, it is hard to find a ideal switch with no leakage current and parasitic capacitor or resistance. Neither a diode nor FET can do. Thus another circuit model with an A.C. current output as shown in Figure 4.10 is proposed. For a steady DC voltage source like battery, the variable capacitance attached will produce an AC current output to the load terminal. Since the charge on the voltage source is blocked by the capacitor, thus the net output power of this circuit is purely provided by the driving vibration. High resolution AC current meter can connected in series to the load terminal to measure the output AC current and verify the performance.

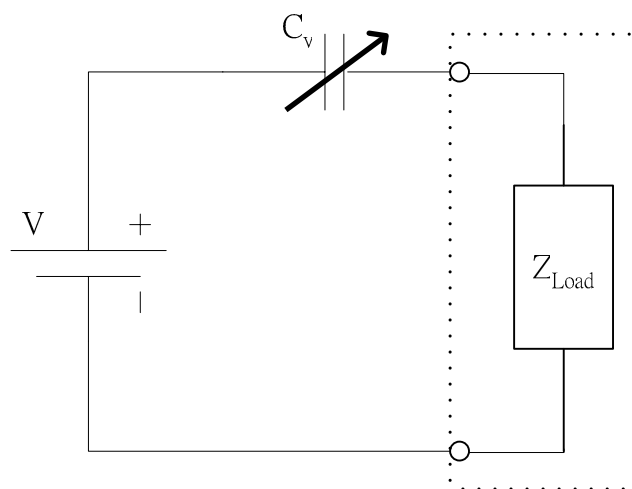


Figure 4.10 Modified application schematic

The predicted AC current with a input voltage 10V is 37.7  $\mu\text{A}$ . However, the actual measured AC current was too small to be measured by the 7.5 digit Keithley 2001 Multimeter. This result is due to several issues. First, the devices with attached mass are very fragile to vertical shocks and all of them were broken before or during the electrical measurements. A device without the attached mass was vibrated successfully as in the mechanical measurement. The same device was tested in the electrical measurement. However, the maximum displacement available was about 10  $\mu\text{m}$  and the capacitance difference was too small to generate an AC current to be measured. The large parasitic capacitance also significantly reduces the AC current generated. Besides, the parasitic resistance in parallel to the capacitance as shown in Figure 4.11 gives a low impedance path and most of the current will flow through it. The parasitic capacitance can be eliminated by connecting the center plate to the substrate. But the parasitic resistance is a serious problem.

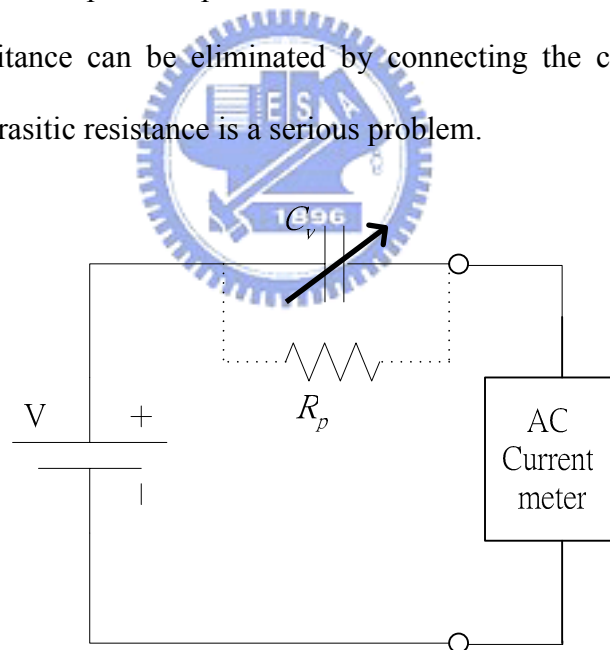


Figure 4.11 Current measurement setup

The reason of the parasitic capacitor has been explained in last section, but the influence of parasitic resistance is more critical. The oxide layer in the SOI wafer provides a good electrical isolation between anchors and pads. The fingers were double checked that all shorted fingers are removed by probe. The coated aluminum of  $5000\text{\AA}$  is decreased to  $3000\text{\AA}$  to prevent the shortage. However, the parasitic resistance is obtained on every measured die. The only possible path is the particles in the gap between the released movable parts and anchors, as Figure 4.12. As mentioned in Chapter 3, after the dicing of the first SOI wafer, comb fingers were destroyed by the cooling water. The broken pieces are all over the gap as shown in Figure 4.13.

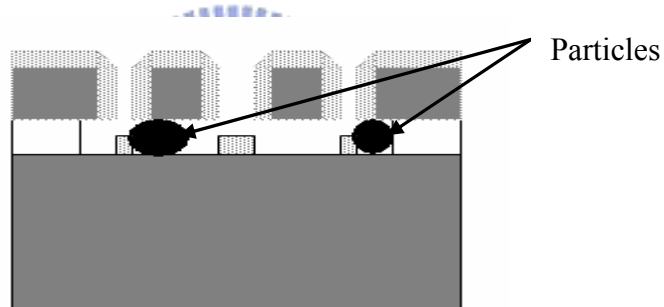


Figure 4.12 Particles making parasitic resistance

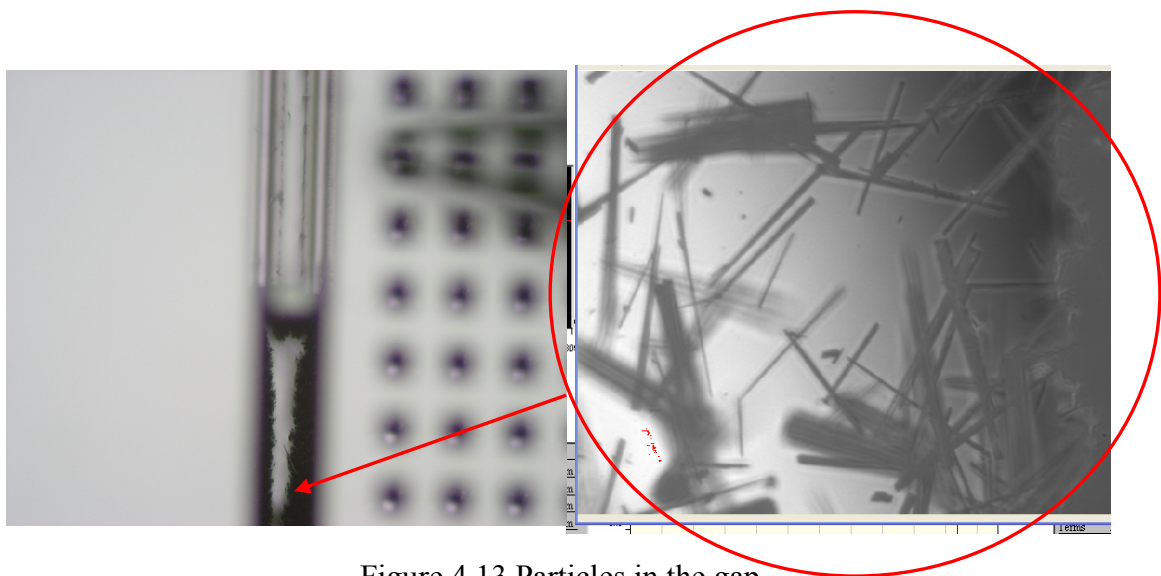


Figure 4.13 Particles in the gap

On the second wafer, fingers were protected by the photoresist. The damage is small. However, after the releasing process, particles still can be found between fingers and on the substrate. One possible source of the particles is from the deep RIE process. As mentioned, the deep RIE process is a series of etching and passivation process. The reactants are removed by the gas flow. Reactants or particles may fall and remain on the substrate after the process. Since the fingers are long and fragile, it is hard to clean the particles by strong air flow or DI water flushing.

The best solution to remove the particles below is to remove the substrate under the movable parts by back etching. Thus, to reduce both the parasitic capacitance and parasitic resistance, the back side substrate etching is preferred.

### 4.3 Output power measurement

The output power measurement based on the schematic in Figure 4.10 was unsuccessful due to the AC current generated was too small to be measured. The output power on resistive load can be estimated by the equation  $P=I^2R_L$  where  $R_L$  is the load resistance and  $I$  is the RMS value of the AC current. The ideal output power with a load  $R_L = 50K\Omega$  is  $35.5 \mu W$  with the calculated AC current with peak current  $37.7 \mu A$ .